RSC Advances

PAPER

View Article Online
View Journal | View Issue

Check for updates

Cite this: *RSC Adv.*, 2021, **11**, 18026

Eco-friendly synthesis of chromeno[4,3-*b*] chromenes with a new photosensitized WO_3/ZnO@NH_2-EY nanocatalyst†

Zahra Jalili, Reza Tayebee* and Farrokhzad M. Zonoz

A new heterogeneous photoredox nanocatalyst WO_3/ZnO@NH_2-EY (EY: eosin Y) was fabricated and characterized employing some instrumental techniques such as XRD, FT-IR, ICP, TGA, and SEM. The photocatalytic efficiency of the prepared material was investigated in the preparation of various chromeno[4,3-*b*]chromenes *via* a simple and practical method. The chromene derivatives were prepared through the condensation of aromatic aldehydes, dimedone, and coumarin under an open-air atmosphere in the presence of a green LED under solventless conditions. The significant advantages of this new method include low reaction time, easy work-up, cost-effective, wide substrate scope, excellent yield, and complete atom economy of the final products. Moreover, the prepared photocatalyst could be frequently recovered up to four times with only a little decrease in the catalytic activity. Furthermore, the progress of the condensation reaction is demonstrated to occur *via* a radical mechanism, which shows that reactive species such as $^{\bullet}O_2^-$ and $OH^{\bullet}$ together with h^+ would be involved in the photocatalytic process. Stability and reusability studies also warranty good reproducibility of the nanocatalyst for at least 4 runs. Eventually, a hot filtration test ensured that the nanohybrid catalyst is stable in the reaction medium and its catalytic activity originates from the whole undecomposed conjugated composite.

Received 16th November 2020
Accepted 29th April 2021

DOI: 10.1039/d0ra09737c

rsc.li/rsc-advances

Open Access Article. Published on 18 May 2021. Downloaded on 2/11/2026 11:12:10 PM.
This article is licensed under a Creative Commons Attribution-NonCommercial 3.0 Unported Licence.

1 Introduction

Multi-component reactions have been known to be powerful tools over conventional multi-step reactions and have emerged as a novel promotion in organic synthesis.[1,2] These reactions offer a direct fast route and enable the assembly of highly complicated and diversified molecules in a one-pot single-step process with enhanced atom economy.[3–7] Chromenes are crucial oxygenated compounds with different biological activities such as antihypertensive,[8] antioxidative,[9] antitumor,[10] antiviral,[11] antibacterial,[12] antileishmanial,[13] anti-tubulin,[14] and anticoagulant,[15] and enable to turn on potassium channels to inhibit dihydrofolate reductase and phosphodiesterase.[16] In the area of anti-cancer chemotherapy, 4*H*-chromenes have been known as a new class of molecules that bind to Bcl-2 anti-apoptotic proteins and promote the apoptotic processes in the cancerous cells.[17–20] Therefore, novel chromenes should be further progressed as potential therapeutic species against cancer cell lines such as glioma, liver, melanoma, and prostate.[19] In addition, the utilization of chromenes is well known in industrial areas such as pigments, biodegradable agrochemicals, cosmetics, optical brightener, fluorescence markers, and laser dyes.[21–23]

Considering the emerging properties of chromene derivatives, the progress of advanced, clean, and uncomplicated methodologies for the efficient catalytic synthesis of these compounds with accessible reagents is of great importance. Some routes have been reported for the synthesis of chromeno [4,3-*b*]chromenes by the reaction of cyclic-1,3-dicarbonyl compounds, arylaldehydes, and 4-hydroxycoumarine in the presence of $SnCl_2 \cdot 2H_2O$,[24] ZnO nanoparticles,[25] $Mg(ClO_4)_2$,[26] molybdic acid-magnetic nanoparticles,[27] *p*-toluene sulfonic acid,[28] nano-$CuFe_2O_4$@SO_3H,[29] I_2/HOAc,[30] heteropolyacids,[31] and Zn (L-proline)$_2$.[32]

Although most of the reported routes have some benefits, however, some disadvantages are also combined with many of them using environmentally toxic organic solvents, expensive mediators, long reaction time, corrosive nature, tedious work-up, non-recyclable catalysts, limited substrate scope, high temperature, and low yields. Therefore, the development of effective and environmental benign methods is desirable for the synthesis of chromene compounds.

Sunlight is an accessible, plentiful, and clean energy source for chemical reactions. Photochemical reactions using visible light are attractive areas in organic synthesis, which provide ubiquitous, non-toxic, eco-friendly, sustainable, inexpensive, and a universally available energy source.[33] However, due to the

Department of Chemistry, School of Sciences, Hakim Sabzevari University, Sabzevar, 96179-76487, Iran. E-mail: rtayebee@hsu.ac.ir

† Electronic supplementary information (ESI) available. See DOI: 10.1039/d0ra09737c

© 2021 The Author(s). Published by the Royal Society of Chemistry

Open Access Article. Published on 18 May 2021. Downloaded on 2/11/2026 11:12:10 PM.
This article is licensed under a Creative Commons Attribution-NonCommercial 3.0 Unported Licence.

increasing attention on the usage of green platforms in organic synthesis, scholars are trying to redesign the synthetic methods by means of visible light.[34–37] Visible light involves a major part of the arriving solar radiation, which can be used to drive various photochemical transformations. Since most organic compounds do not absorb visible light, the application of photochemical reactions has been restricted. Therefore, the development of new and efficient visible light photocatalysts towards chemical transformations is a necessity. Photoredox catalysts absorb visible light to provide the required energy to initiate a photochemical reaction. Among metal-free organic dyes, EY has been used as an economic and environment-friendly alternative to many transition metal photoredox catalysts.

The photochemistry of EY has been well examined *via* excitation by visible light and this molecule goes through a fast intersystem crossing to the lowest energy states.[38] EY can easily absorb green light; therefore, various applications have emerged for this organic photosensitizer in visible light-promoted organic synthesis.[39–41] However, because EY has harmful effects on the environment, a solution is required. One of the most efficient ways to solve this problem is to prepare a heterogeneous catalyst from this material using suitable catalytic substrates. There is an example of the heterogenization of EY on TiO_2 and its application in the degradation of diclofenac *via* the solar activation of titanium dioxide.[42] In addition, a new metal–organic framework photocatalyst modified by EY "EY@UiO-66-NH_2" has been synthesized and used in the C–H activation of tertiary amines.[43] Also, the reduction of 4-nitrophenol has been achieved by handling solar irradiation under green conditions by utilizing an effective polymer-supported EY photocatalyst.[44] Further transformations involving oxidation of thioethers and phenylboronic acids[45] as well as C–C and C–P coupling reactions[46] were also performed by EY-supported photocatalysts.

As far as we know, semiconducting metal oxides have a very crucial impact in a wide domain of chemical industries such as lithium ion batteries,[47] sensors,[48] optoelectronics,[49] and photocatalysts.[50] Among various types of these semiconductors, zinc oxide and tungsten(VI) oxide are very appropriate to be applied as photocatalysts because of their proper bandgap (3.2–3.35 eV).[51] However, semiconductor composites can improve the electron transitions between the $(e^-)/(h^+)$ pairs in the large energy gaps and can be regarded as effectual photocatalysts.[52] To date, ZnO-WO_3,[53] CuO/WO_3/TiO_2,[54] ZnO–TiO_2,[55] and ZnO/CeO_2 (ref. 56) are prepared and used as effective photocatalysts in a number of routine transformations under visible light irradiation.

In the extension of our previous studies on the development of green synthetic protocols to achieve important heterocyclic compounds[57–59] and to recognize the extensive applications of chromene derivatives, herein, we report a simple and convenient new method to synthesize different substituted chromeno [4,3-*b*]chromene derivatives by means of a green LED through

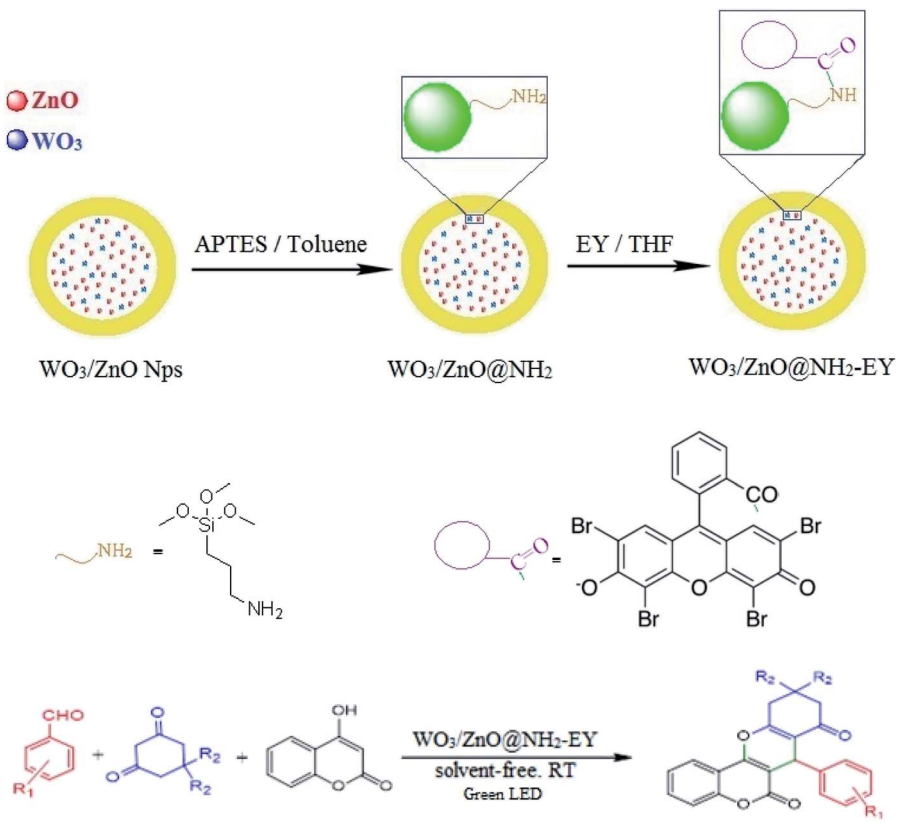

Scheme 1 A general route for the preparation of different substituted chromeno[4,3-*b*]chromenes.

Open Access Article. Published on 18 May 2021. Downloaded on 2/11/2026 11:12:10 PM.
This article is licensed under a Creative Commons Attribution-NonCommercial 3.0 Unported Licence.

the multicomponent condensation of aryl aldehydes, 1,3-cyclohexanedione, and 4-hydroxylcoumarin, using an EY-supported nanocomposite (WO_3/ZnO) as a green heterogeneous nanocatalyst under solventless conditions (Scheme 1).

The interaction of EY with the solid support material can occur *via* three routes including hydrophobic, hydrogen bond, and Lewis acid–base interactions. The hydrophobic interaction refers to the adsorption affinity of EY *via* its non-hydrophobic functional groups. This interaction is not too strong, however, it should be considered. Hydrogen bonding also widely happens in the adsorption of this polar compound to the support material through the lone-pair hydrogen bonding donors on EY with the acceptor sites on the support. Finally, Lewis acid–base interaction occurs *via* the carboxyl group of EY with the basic sites such as the pendant amino group of the alkyl chain. Therefore, all of the above interactions could be regarded as electronic interactions between EY and WO_3/ZnO@NH_2.[60–63] However, precise adsorption isotherm experiments are necessary to elucidate the exact mechanism of adsorption.

2 Experimental section

2.1 Materials and methods

All chemicals including zinc chloride, sodium hydroxide, zinc acetate, sodium tungstate, EY, benzaldehyde, dimedone, 4-hydroxycoumarin, (3-aminopropyl)triethoxysilane (APTES), and solvents were purchased from Sigma-Aldrich, Merck, and Fluka, and utilized as received without further purification. The morphology of the synthesized nanophotocatalyst was studied by a Mira 3-XMU field emission scanning electron microscope (FE-SEM). ^{1}H- and ^{13}C-NMR spectra were recorded on a 300 MHz Bruker AVANCEC III spectrometer using TMS as the internal reference. Melting points were attained on a Stuart BI Branstead Electrothermal IA9200 apparatus. Fourier transform infrared (FT-IR) spectra were recorded on a Shimadzu 8700 Fourier transform spectrometer in the range of 400–4000 cm^{-1} with KBr pellets. UV-visible spectra were obtained using a Photonix UV-visible array spectrophotometer. X-ray diffraction patterns (XRD) were attained on an Xpert MPD diffractometer with Cu K_α radiation at 30 mA and 40 keV and a scanning rate of 3° min^{-1} in the 2θ domain from 5° to 80°. Thermogravimetric analysis was carried out with a TGA 92 Setaram at 10 °C min^{-1}. The chemical composition of the catalyst was determined by an inductively coupled plasma spectrometer (ICP-MS; model VARIAN VISTA-PRO).

2.2 Preparation of WO_3/ZnO nanoparticles

About 30 mL NaOH (4 M) was added drop-wise into a 20 mL mixture of zinc acetate (1 M) and 2 mL of $Na_2WO_4 \cdot 2H_2O$ (0.5 M). Then, the produced suspension remained at room temperature under mild stirring for 3 h to generate the desired precursor. Thereafter, the obtained suspension was subsequently transferred to a 250 mL ground-glass stopped conical flask and aged at 95 °C for 10 h. Finally, the deposited precipitate at the bottom of the conical flask was gathered, completely washed with water, and air-dried under ambient conditions.

2.3 Surface modification of WO_3/ZnO *via* the anchoring of APTES

800 mg WO_3/ZnO was dispersed in an anhydrous solution of toluene (60 mL). To this suspension, 1.6 mL APTES was added and the obtained mixture was refluxed for 24 h. Finally, the attained precipitate was filtered and dried in an oven at 60 °C for 12 h.

2.4 Surface modification of WO_3/ZnO@NH_2 with EY

WO_3/ZnO@NH_2-EY was supplied through a well-known wet-impregnation method. According to this procedure, 20×10^{-3} mL EY was dissolved in THF. Then, 0.5 g of WO_3/ZnO@NH_2 was gradually added to this solution for 12 h in a dark atmosphere. Eventually, the resulting precipitate was dried at 80 °C under air for 24 h.

2.5 A general procedure for the synthesis of substituted chromeno[4,3-*b*]chromene

Benzaldehyde (100 mg, 1 mmol), dimedone (140 mg, 1 mmol), 4-hydroxycoumarin (162 mg, 1 mmol), and the desired amount of WO_3/ZnO@NH_2-EY (30 mg) were successively added to a test tube equipped with a magnet. Then, the reaction mixture was irradiated with a green light-emitting diode ($\lambda_{max} = 535$ nm) at room temperature in an open-air atmosphere and completion of the reaction was monitored by TLC (*n*-hexane : ethyl acetate, 3 : 1). After completion of the reaction, the mixture was quenched with H_2O (3 mL) and the desired chromene product was dissolved in EtOAc. Then, the EtOAc layer was removed and the aqueous fraction was again extracted with EtOAc (3×3 mL). Finally, the attained organic layer was dried over sodium sulfate and concentrated *in vacuo*. The crude accomplished product was purified through column chromatography (100–200 mesh silica gel; EtOAc/hexane) to afford the pure chromene.

2.6 Spectral data

2.6.1 10,10-Dimethyl-7-phenyl-10,11-dihydrochromeno[4,3-*b*]chromene-6,8(7*H*,9*H*)-dione (Table 4, entry 1). ^{1}H NMR (300 MHz, DMSO-d_6); δ: 7.83 (1H, d, $J = 7.8$ Hz), 7.53 (1H, d, $J = 7.2$ Hz), 7.05–7.35 (7H, m), 4.69 (1H, s), 2.66 (2H, s), 2.24 (1H, d, $J = 15.9$ Hz), 2.12 (1H, d, $J = 16.2$ Hz), 1.07 (3H, s), 0.97 (3H, s) ppm; ^{13}C NMR (75 MHz, DMSO-d_6); δ: 195.8, 162.6, 160.2, 154.0, 152.4, 143.0, 132.7, 128.7, 128.3, 127.0, 124.7, 122.8, 116.5, 114.5, 113.5, 106.3, 50.6, 33.4, 32.3, 29.0, 27.3 ppm.

2.6.2 10,10-Dimethyl-7-(4-nitrophenyl)-10,11-dihydrochromeno[4,3-*b*]chromene-6,8(7*H*,9*H*)-dione (Table 4, entry 2). ^{1}H NMR (300 MHz, DMSO-d_6); δ: 8.00 (2H, d, $J = 8.7$ Hz), 7.89 (1H, s), 7.84 (1H, d, $J = 7.8$ Hz), 7.55 (1H, d, $J = 7.2$ Hz), 7.47 (1H, d, $J = 8.7$ Hz), 7.34 (1H, t, $J = 7.5$ Hz), 7.26 (1H, d, $J = 8.1$ Hz), 4.82 (1H, s), 2.68 (2H, s), 2.24 (1H, d, $J = 16.2$ Hz), 2.11 (1H, d, $J = 16.2$ Hz), 1.07 (3H, s), 0.96 (3H, s) ppm; ^{13}C NMR (75 MHz, MSO-d_6); δ: 195.8, 163.0, 160.2, 154.5, 152.6, 150.2, 146.7, 133.0,

© 2021 The Author(s). Published by the Royal Society of Chemistry

Open Access Article. Published on 18 May 2021. Downloaded on 2/11/2026 11:12:10 PM.
This article is licensed under a Creative Commons Attribution-NonCommercial 3.0 Unported Licence.

129.9, 124.8, 123.4, 122.9, 116.8, 13.6, 113.3, 105.0, 50.5, 33.8, 32.3, 28.9, 27.4 ppm.

2.6.3 10,10-Dimethyl-7-(4-methoxyphenyl)-10,11-dihydrochromeno[4,3-*b*]chromene-6,8(7*H*,9*H*)-dione (Table 4, entry 4). ^{1}H NMR (300 MHz, DMSO-d$_6$); δ: 7.82–7.85 (1H, m), 7.52–7.57 (1H, m), 7.24–7.35 (2H, m), 7.14 (2H, d, J = 9.0 Hz), 7.04 (1H, d, J = 9.0 Hz), 6.62–6.70 (1H, m), 4.66 (1H, s), 3.63 (3H, s), 2.66 (2H, s), 2.16 (1H, d, J = 16.2 Hz), 2.04 (1H, d, J = 16.2 Hz), 1.08 (3H, s), 0.95 (3H, s) ppm; ^{13}C NMR (75 MHz, DMSO-d$_6$); δ: 195.9, 161.5, 160.5, 158.5, 153.6, 152.3, 135.1, 132.5, 129.6, 129.3, 124.6, 122.7, 116.6, 115.6, 113.6, 113.3, 106.3, 55.1, 50.7, 32.3, 32.1, 29.1, 27.3 ppm.

2.6.4 10,10-Dimethyl-7-(3-nitrophenyl)-10,11-dihydrochromeno[4,3-*b*]chromene-6,8(7*H*,9*H*)-dione (Table 4, entry 5). ^{1}H NMR (300 MHz, DMSO-d$_6$); δ: 8.01 (1H, s), 7.87 (1H, d, J = 8.1 Hz), 7.78 (1H, d, J = 7.8 Hz), 7.59 (1H, d, J = 6.6 Hz), 7.49 (1H, t, J = 7.5 Hz), 7.24–7.35 (2H, m), 7.18 (1H, d, J = 8.1 Hz), 4.81 (1H, s), 2.66 (1H, d, J = 18 Hz), 2.58 (1H, d, J = 18 Hz), 2.19 (1H, d, J = 16.5 Hz), 2.08 (1H, d, J = 16.5 Hz), 1.03 (3H, s), 0.93 (3H, s) ppm; ^{13}C NMR (75 MHz, DMSO-d$_6$); δ: 195.6, 163.0, 159.8, 154.1, 152.1, 147.5, 144.7, 135.0, 132.8, 129.4, 124.6, 123.1, 122.7, 121.7, 116.5, 113.0, 104.6, 49.9, 38.8, 33.2, 31.9, 28.4, 26.8 ppm.

2.6.5 7-(3-Nitrophenyl)-10,11-dihydrochromeno[4,3-*b*]chromene-6,8(7*H*,9*H*)-dione (Table 4, entry 6). ^{1}H NMR (300 MHz, DMSO-d$_6$); δ: 7.99–8.02 (2H, m), 7.87–7.90 (2H, m), 7.54–7.60 (1H, m), 7.23–7.45 (3H, m), 5.04 (1H, s), 2.77–2.95 (2H, m), 2.39–2.44 (2H, m), 2.04–2.17 (2H, m), ppm; ^{13}C NMR (75 MHz, DMSO-d$_6$); δ: 195.9, 164.3, 152.7, 144.7, 136.0, 132.7, 129.0, 124.5, 122.8, 122.6, 122.2, 117.0, 115.3, 113.3, 105.4, 36.7, 33.5, 27.1, 20.1 ppm.

2.6.6 7-(4-Methoxyphenyl)-10,11-dihydrochromeno[4,3-*b*]chromene-6,8(7*H*,9*H*)-dione (Table 4, entry 7). ^{1}H NMR (300 MHz, DMSO-d$_6$); δ: 8.04 (1H, d, J = 7.8 Hz), 7.73 (1H, t, J = 7.5 Hz), 7.43–7.54 (2H, m), 7.33 (2H, d, J = 8.4 Hz), 6.87 (2H, d, J = 7.8 Hz), 3.82 (3H, s), 4.87 (1H, s), 2.88–3.06 (2H, m), 2.50 (2H, t, J = 6.3 Hz), 2.15–2.27 (2H, m) ppm; ^{13}C NMR (75 MHz, DMSO-d$_6$); δ: 195.5, 163.3, 160.2, 159.3, 153.4, 152.5, 135.3, 132.6, 129.6, 124.7, 122.8, 120.8, 116.7, 116.1, 113.7, 113.3, 111.7, 106.5, 55.2, 36.9, 32.4, 26.9, 20.2 ppm.

3 Results and discussion

3.1 Characterization and physicochemical properties of WO_3/ZnO@NH_2-EY nanoparticles

The morphology and physicochemical properties of the prepared WO_3/ZnO@NH_2-EY nanocatalyst were investigated by means of FT-IR, SEM, ICP, UV-Vis, and XRD. FT-IR and UV-Vis techniques are the most informative techniques to examine the surface interaction of EY with the surface functional groups of WO_3/ZnO@NH_2.

3.1.1 FT-IR spectroscopy. The FT-IR spectra of the fabricated samples in the range of 400–4000 cm^{-1} are shown in Fig. 1. To ensure the binding of EY on the surface of WO_3/ZnO@NH_2-EY, the FT-IR of all the fragments including WO_3/ZnO (a), WO_3/ZnO@NH_2 (b), EY (c), and WO_3/ZnO@NH_2-EY (d) were studied. This study proved the anchoring of EY onto the

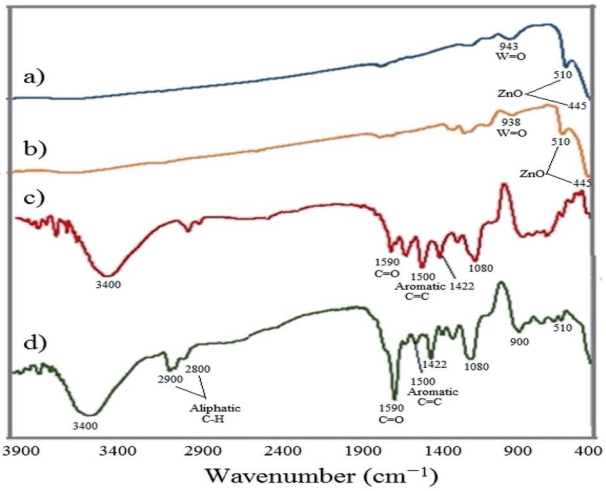

Fig. 1 FT-IR spectra of (a) WO_3/ZnO, (b) WO_3/ZnO@NH_2, (c) EY, and (d) WO_3/ZnO@NH_2-EY.

surface of WO_3/ZnO@NH_2-EY. The typical absorption bands in the region of 400–600 cm^{-1} are due to ZnO species. The FT-IR of WO_3/ZnO and WO_3/ZnO@NH_2 revealed a strong absorption band at ~445 cm^{-1} with a shoulder at ~510 cm^{-1} corresponding to the Zn–O stretching vibrations. Moreover, the weak bands at 943 and 948 cm^{-1} are related to W=O bonds in the octahedral WO_3.[64,65] The grafting of the amine group on the surface of WO_3/ZnO can be approved by the observation of the corresponding aliphatic bands in 2900 and 3400 cm^{-1}.[66] The appearance of the EY characteristic bands in the FT-IR of WO_3/ZnO@NH_2-EY proved that the structure of EY is unchanged after immobilization. The FT-IR spectrum of WO_3/ZnO@NH_2-EY was also compared to that of the parent EY. The observation of the absorption bands at 1590 and 1500 cm^{-1} due to the

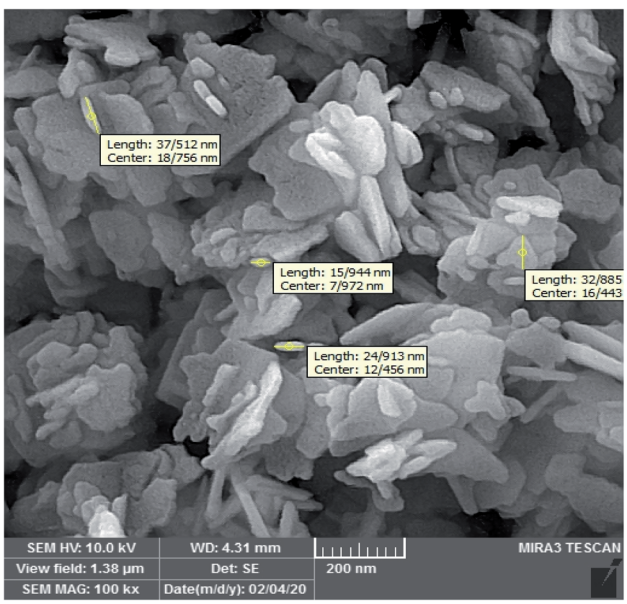

Fig. 2 The FE-SEM images of WO_3/ZnO@NH_2-EY.

Open Access Article. Published on 18 May 2021. Downloaded on 2/11/2026 11:12:10 PM.
This article is licensed under a Creative Commons Attribution-NonCommercial 3.0 Unported Licence.

carboxyl functional group and the C=C of aromatic phenyl rings, respectively, unambiguously confirmed the loading of EY onto the surface of the WO_3/ZnO@NH_2 framework.[67,68] However, there were no detectable peaks due to the WO_3 species and it seems that a little surface segregated WO_3 had no apparent effects on the infrared spectrum of ZnO nanoparticles.

3.1.2 FESEM of WO_3/ZnO@NH_2-EY. The surface morphology of WO_3/ZnO@NH_2-EY was further studied by FE-SEM (Fig. 2). From this figure, it can be concluded that the prepared nanocatalyst has an approximately nanosheet framework. Moreover, the diameter of these nanosheets was about 25–35 nm. In addition, the FE-SEM images of WO_3/ZnO@NH_2-EY with 5 mm particle size were achieved to investigate the distribution of tungsten and zinc (Fig. 3).[69] As can be seen from these pictures, the presence and steady distribution of these elements in the WO_3/ZnO@NH_2-EY nanocatalyst can be easily proven.

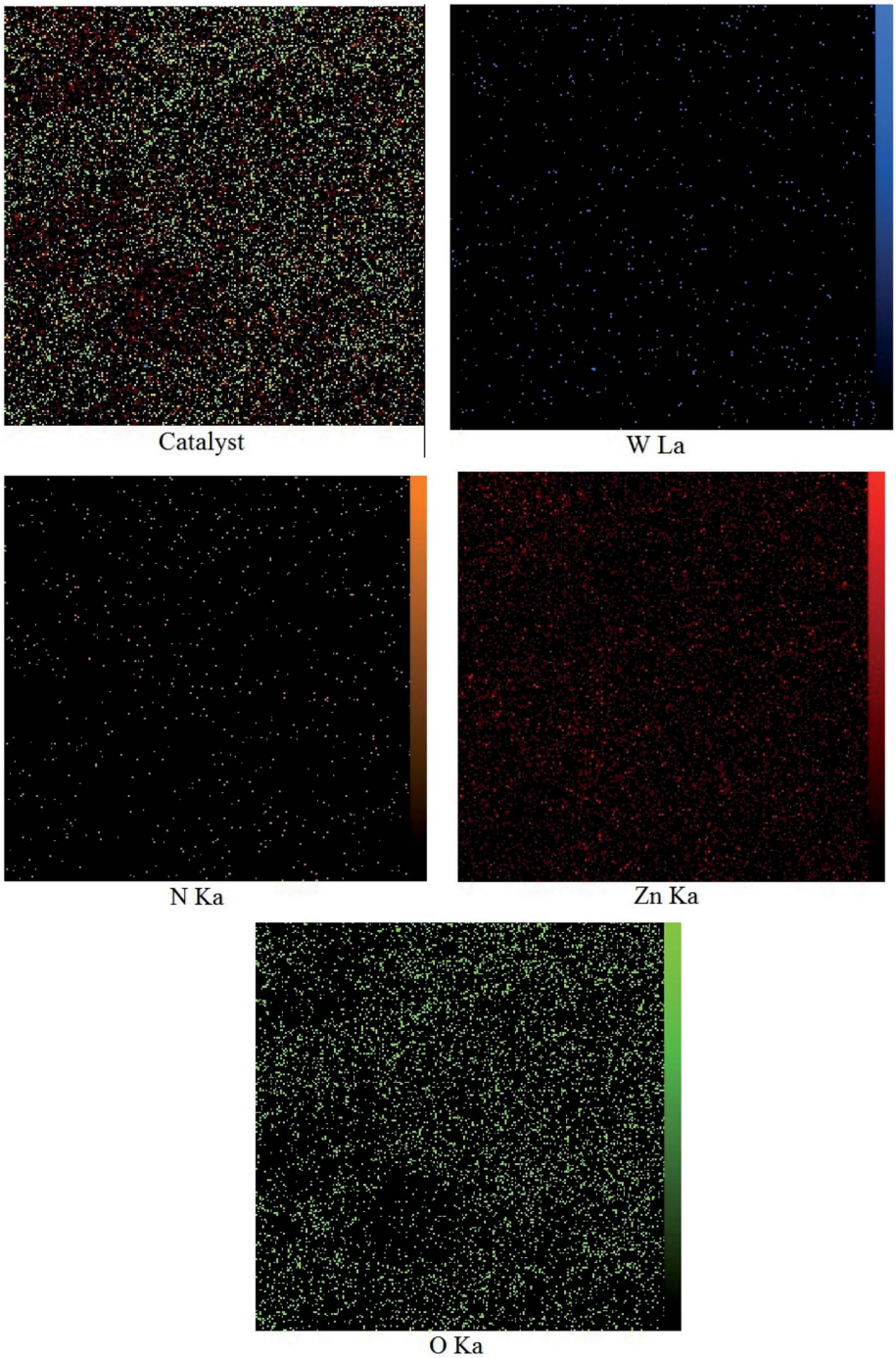

Fig. 3 The FE-SEM map pictures of WO_3/ZnO@NH_2-EY.

© 2021 The Author(s). Published by the Royal Society of Chemistry

Open Access Article. Published on 18 May 2021. Downloaded on 2/11/2026 11:12:10 PM.
This article is licensed under a Creative Commons Attribution-NonCommercial 3.0 Unported Licence.

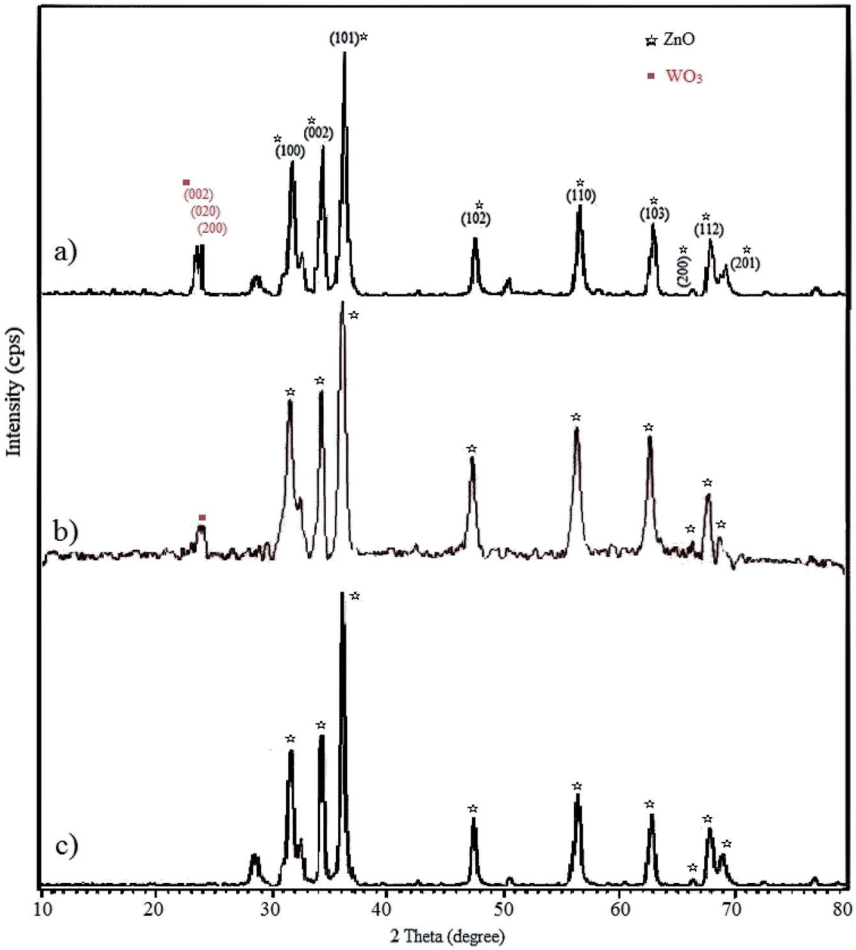

Fig. 4 Wide-angle XRD pattern of (a) WO_3/ZnO, (b) WO_3/ZnO@NH_2, and (c) WO_3/ZnO@NH_2-EY.

3.1.3 XRD. The crystallinity of the fabricated WO_3/ZnO, WO_3/ZnO@NH_2, and WO_3/ZnO@NH_2-EY was explored through wide-angle XRD (Fig. 4). In the XRD pattern of WO_3/ZnO, obvious diffraction peaks at the 2θ of 23.1°, 23.7°, and 24.2° corresponded to the (002), (020), and (200) crystal planes of WO_3, respectively, which appeared as broad peaks.[70] However, there were no detectable peaks related to WO_3 in the XRD pattern of WO_3/ZnO@NH_2-EY due to its low amount or amorphous nature on the surface of ZnO. The diffraction patterns of the synthesized WO_3/ZnO@NH_2-EY showed that the material is a crystalline material and major parts of the XRD pattern were fitted well with the standard data of the ZnO structure. Low-intensity peaks at the 2θ of 31.6, 34.4, 36.3, 47.6, 56.7, 62.9, 66.3, 67.8, 69.1, 72.6, and 76.9° corresponded to the (100), (002), (101), (102), (110), (103), (200), (112), (201), (004), and (202) planes, respectively. These results confirmed that WO_3/ZnO@NH_2-EY has a very close topology to ZnO.[68] Moreover, the half-value crystallite scale can be calculated using the XRD data in the Debye–Scherrer formula; thus, the half-value crystallite scale of WO_3/ZnO@NH_2-EY was attained as ~31 nm, which is in accordance with the FESEM results.

3.1.4 TGA. The thermal stability of the WO_3/ZnO@NH_2-EY nanophotocatalyst was explored by TGA (Fig. 5). It seems that a little weight-gain at the temperature of about 40 °C would be due to the differences in the thermal conductivity and the heat capacity of the purging gas.[71] Following the graph, three stages of decomposition can be seen. The first gradual weight-loss of about 1.79% was observed below 180 °C, which is most likely due to water desorption from the surface of nanoparticles and

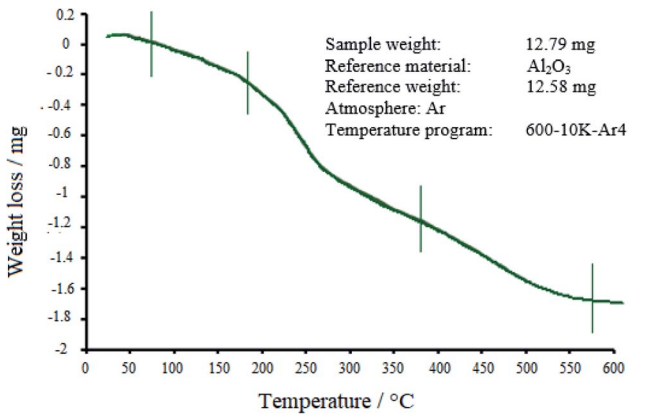

Fig. 5 TGA profile for WO_3/ZnO@NH_2-EY.

Open Access Article. Published on 18 May 2021. Downloaded on 2/11/2026 11:12:10 PM. This article is licensed under a Creative Commons Attribution-NonCommercial 3.0 Unported Licence.

loss of moisture content.[72] Then, the EY moiety started to be destroyed at about 200–380 °C with an average weight loss of about 6.64%. Further weight loss (4.37%) at higher temperatures would probably be due to the burning of alkyl-chain remnants, which was accompanied by the crystallization of ZnO and WO_3 up to 500 °C.

3.1.5 UV-vis and ICP. The amount of EY loaded onto WO_3/ZnO@NH_2 was monitored by UV-vis spectroscopy of the solution involving EY during the immobilization process. To achieve the degree of loaded EY, the UV-vis spectra of the solutions of WO_3/ZnO@NH_2 were attained before and after the addition of EY. Thus, 0.5 g of WO_3/ZnO@NH_2 was suspended in 5 mL THF solution having 100 mg of EY. Then, the heterogeneous suspension was stirred for 7 h (Fig. 6). Obviously, most of the EY content was adsorbed on the surface of WO_3/ZnO@NH_2 after 5 h. However, the amount of EY loaded onto to the surface of the solid material was precisely detected by ICP and the weight% of 15 was attained. It means that ~0.21 mmol of EY was grafted per gram of the WO_3/ZnO@NH_2 photocatalyst. Thus, most of the vanished EY (as documented by the UV-vis study) was physisorbed onto the surface of the photocatalyst.

3.2 Catalytic tests

To achieve the best reaction conditions, we performed a model condensation reaction using benzaldehyde (1 mmol), dimedone (1 mmol), and 4-hydroxycoumarin (1 mmol) in the presence of WO_3/ZnO@NH_2-EY (0.03 g) under solventless conditions. Then, the reaction mixture was irradiated with a green light-emitting diode (λ_{max}, 535 nm) at room temperature in an open-air container. Thereafter, the desired chromeno[4,3-*b*]chromene was formed in good yield after 45 min (Table 1). This study demonstrated that if we remove any of the aforementioned requirements such as EY, WO_3/ZnO@NH_2-EY, and LED, the reaction yield will be significantly diminished.

3.2.1 Studying the effect of the catalyst amount. Herein, the reactions were performed with different amounts of the catalyst in order to optimize the exact quantity of WO_3/ZnO@NH_2-EY. As seen in Fig. 7, 0.03 g of WO_3/ZnO@NH_2-EY was appropriate and gave 97% yield under the selected reaction conditions. However, a further increment of the catalyst amount affected neither the yield% nor the reaction time, while a lower yield of the desired product was attained on decreasing the catalyst amount (Fig. 7).

3.2.2 Effect of different solvents. In this step, we shifted our focus on the impact of the solvent in the reaction progress (Table 2). Thus, the condensation of dimedone, benzaldehyde, and 4-hydroxycoumarin under optimum conditions was performed with some selected solvents such as CH_3CN, THF, toluene, and ethanol. According to the obtained data in Table 2,

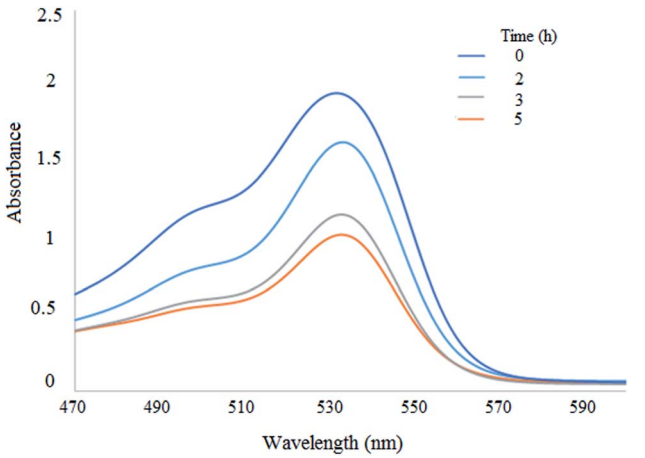

Fig. 6 UV-vis spectral changes under the loading of EY on WO_3/ZnO@NH_2.

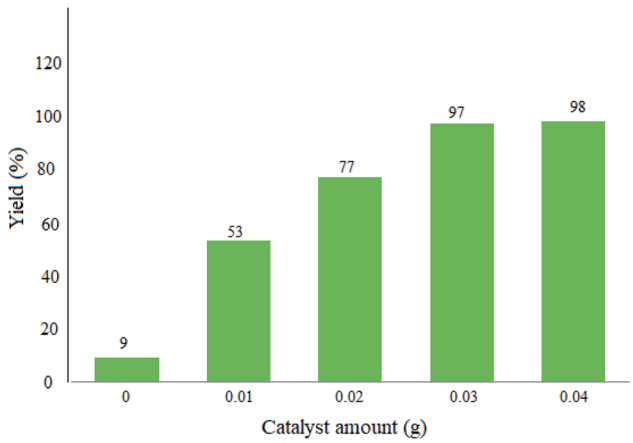

Fig. 7 Effect of the catalyst amount on the condensation of dimedone, benzaldehyde, and 4-hydroxycoumarin under the selected reaction conditions below Table 1 in the presence of a green LED (25 W, λ = 535 nm) after 45 min.

Table 1 Optimization of the reaction conditions for the condensation of dimedone, benzaldehyde, and 4-hydroxycoumarin[a]

Entry	Light	Light source	WO_3/ZnO@NH_2-EY (g)	Time (min)	Yield (%)
1	—	—	—	45	4
2	Green LED	25 W, λ = 535 nm	—	45	9
3	Dark	—	0.03	45	43
4	White LED	20 × 1 W	0.03	45	55
5	Green LED	25 W, λ = 535 nm	0.03	45	97

[a] Reaction conditions: dimedone (1.0 mmol), benzaldehyde (1.0 mmol), and 4-hydroxycoumarin (1.0 mmol) under solvent-free conditions in an open-air atmosphere at room temperature.

© 2021 The Author(s). Published by the Royal Society of Chemistry

Open Access Article. Published on 18 May 2021. Downloaded on 2/11/2026 11:12:10 PM.
This article is licensed under a Creative Commons Attribution-NonCommercial 3.0 Unported Licence.

Table 2 Optimization of the solvent on the condensation of dimedone, benzaldehyde, and 4-hydroxycoumarin using a green LED (25 W)[a]

Entry	WO_3/ZnO@NH_2-EY (g)	Solvent	Time (min)	Yield (%)
1	0.03	—	45	97
2	0.03	H_2O	180	45
3	0.03	Toluene	180	62
4	0.03	Ethanol	180	77
5	0.03	CH_3CN	180	95

[a] Reaction conditions are described below Table 1. 3 mL solvent was used.

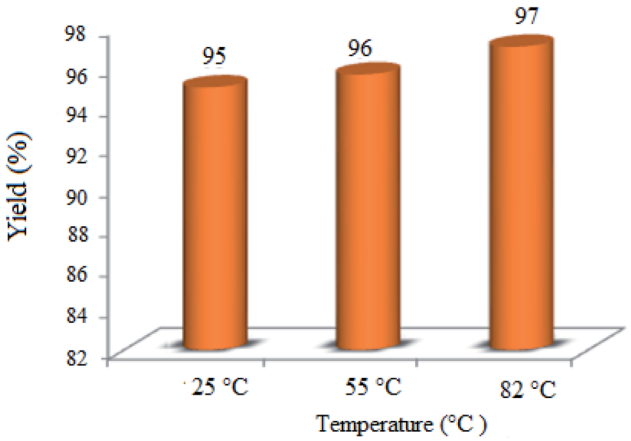

Fig. 8 Effect of the temperature on the condensation of dimedone, benzaldehyde, and 4-hydroxycoumarin in the presence of 0.03 g of WO_3/ZnO@NH_2-EY, green LED, and CH_3CN (3 mL). The reaction time was selected as 3 h.

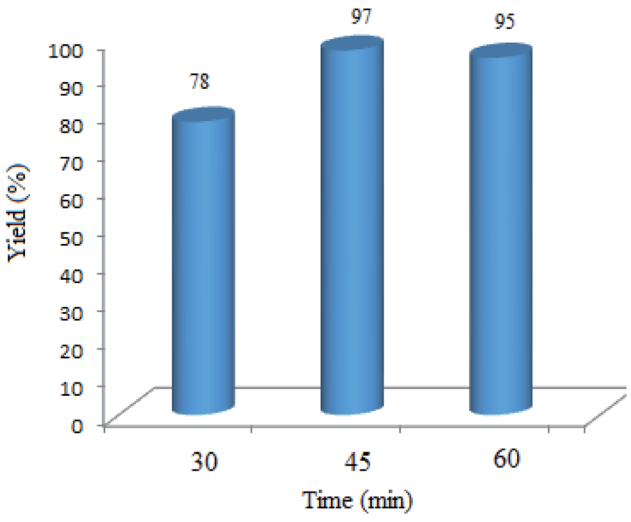

Fig. 9 Effect of the reaction time on the condensation of dimedone, benzaldehyde, and 4-hydroxycoumarin. Green LED (25 W) was used under solvent-free conditions in an open atmosphere at room temperature.

the solvent-free condition was the best choice between the tried solvents and provided the maximum yield of 97% after 45 min.

3.2.3 Effect of the reaction temperature. The impact of the reaction temperature was speculated in the condensation of dimedone, benzaldehyde, and 4-hydroxycoumarin to achieve the best reaction conditions (Fig. 8). Interestingly, the yield% was only a little affected by the reaction temperature and the best result was attained at RT (~25 °C) after 3 h. Therefore, the temperature of 25 °C was the optimum temperature for all the runs.

3.2.4 Effect of the reaction time. The effect of the reaction time was investigated to explore the minimum time needed to acquire the best yield. As Fig. 9 shows, 45 min was adequate to reach the maximum yield of 97%. Noteworthily, a little decrease in the yield% was attained by extending the reaction time, which would be due to the poisoning of the catalyst surface. The above experiments declared that the best condition can be solvent-free under an open air atmosphere at room temperature in the presence of 0.03 g of the WO_3/ZnO@NH_2-EY nanocatalyst.

Table 3 Studying the catalytic activity and some contributing experimental parameters on the condensation of dimedone, benzaldehyde, and 4-hydroxycoumarin[a]

Entry	Green LED (25 W, λ = 535 nm)	Catalyst	Air	Time (min)	Yield (%)
1	+	—	+	45	9
2	+	EY	+	45	72
3	+	WO_3/ZnO@NH_2	+	45	42
4	+	WO_3/ZnO@NH_2-EY	+	45	97
5	–	WO_3/ZnO@NH_2-EY	+	45	43
6	+	WO_3/ZnO@NH_2-EY	N_2	45	18

[a] Reaction conditions are described below Table 1. 0.03 g of the catalyst was used under solvent-free conditions.

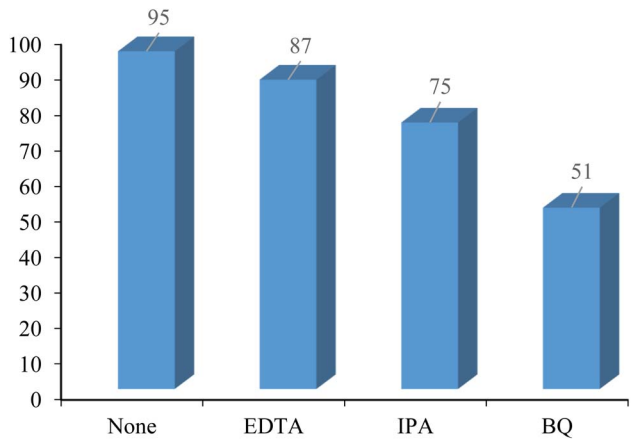

Fig. 10 Effect of some familiar scavengers on the reaction progress under the standard reaction conditions described below Table 1.

Open Access Article. Published on 18 May 2021. Downloaded on 2/11/2026 11:12:10 PM.
This article is licensed under a Creative Commons Attribution-NonCommercial 3.0 Unported Licence.

Table 4 Substrate scope for the condensation of dimedone, benzaldehyde, and 4-hydroxycoumarin[a]

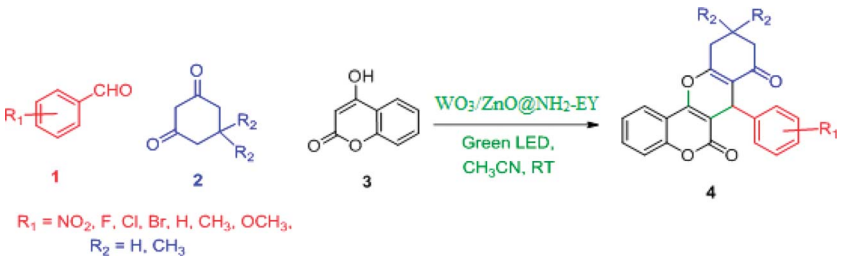

Aldehyde	Dimedone	Product	Yield (%), select. (%)	TON[b]	TOF[c]	M.P.
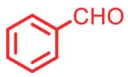	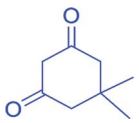	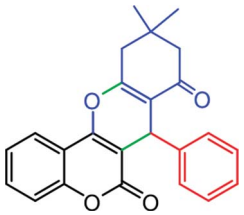	97, (98)	29.66	39.5	220–222 (ref. 78)
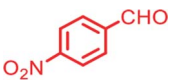	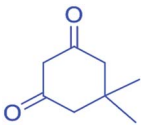	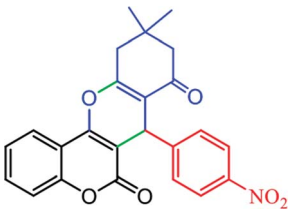	91, (85)	30.33	40.44	208–210 (ref. 28)
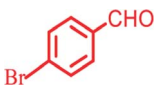	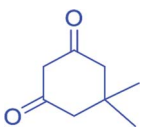	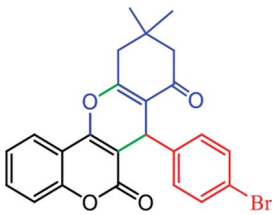	73, (94)	24.33	32.44	228–230 (ref. 28)
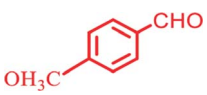	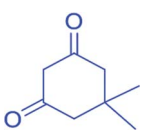	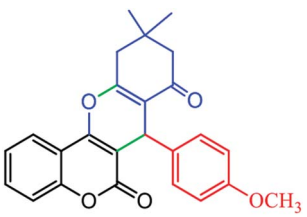	72, (96)	24	32	187–189 (ref. 78)
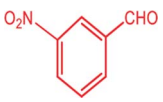	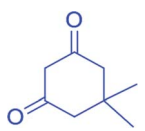	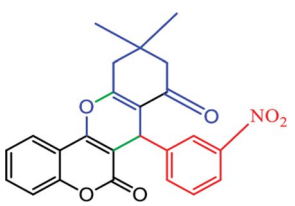	73, (88)	24.33	32.44	240–245 (ref. 79)
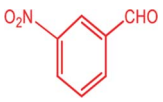	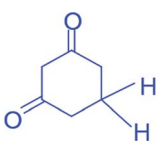	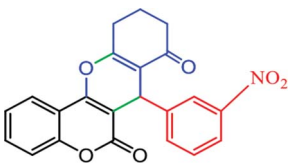	76, (92)	25.33	33.78	218–220 (ref. 80)

© 2021 The Author(s). Published by the Royal Society of Chemistry

Open Access Article. Published on 18 May 2021. Downloaded on 2/11/2026 11:12:10 PM. This article is licensed under a Creative Commons Attribution-NonCommercial 3.0 Unported Licence.

Table 4 (*Contd.*)

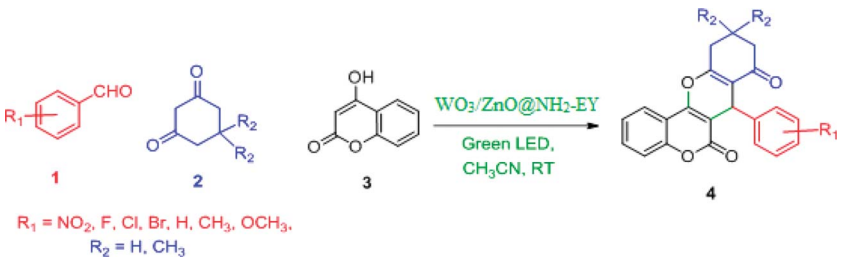

Aldehyde	Dimedone	Product	Yield (%), select. (%)	TON[b]	TOF[c]	M.P.
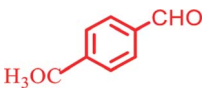	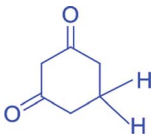	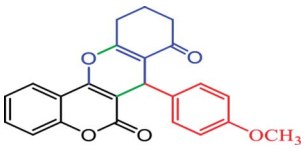	78, (97)	26	34.67	196–197 (ref. 81)

[a] Reaction conditions are described below Table 1. Green LED (2.5 W, λ = 535 nm) under solvent-free conditions in air at room temperature. Reaction time was 45 min and 0.03 g of WO_3/ZnO@NH_2-EY was used in all the cases. [b] TON is calculated based on the moles of the converted substrate/mol of the catalyst. [c] TOF = (yield/time (h))/catalyst amount (g).

Table 5 The comparison of the catalytic activity of WO_3/ZnO@NH_2-EY with some reported catalysts in the synthesis of chromeno[4,3-*b*] chromene[a]

Catalyst	Catalyst amount	Time (h)	Temp (°C)	Solvent	Yield (%)
$Fe(DS)_3$	10 mol%	1.5	70	H_2O (2.5 mL)	90 (ref. 76)
Fe_3O_4@SiO_2@$(CH_2)_3OMoO_3H$	0.002 g	0.75	80	—	90 (ref. 27)
Nano-$CuFe_2O_4$@SO_3H	(0.05 g)	2.5	70	EtOH (5 mL)	90 (ref. 29)
t-ZrO_2 np	10 mol%, 12.3 mg	0.5	80	H_2O (5 mL)	91 (ref. 82)
Eozin Y	2 mol%	3.5	r.t green LED	CH_3CN (3 mL)	77 (ref. 83)
WO_3/ZnO@NH_2-EY	30 mg (~0.21 mmol EY per g of photocatalyst)	0.75	r.t. green LED	—	97 (this work)

[a] Reaction conditions are described below Table 1.

3.2.5 Effect of the light source, presence of oxygen, and EY on the reaction progress. The catalytic activity of EY, WO_3/ZnO@NH_2, and WO_3/ZnO@NH_2-EY nanoparticles was separately investigated for the condensation of dimedone, benzaldehyde, and 4-hydroxycoumarin under the standard reaction conditions (Table 3). This investigation demonstrated that the condensation reaction is greatly dependent on the presence of light and oxygen. In addition, the best yield was attained with the nanocomposite WO_3/ZnO@NH_2-EY and WO_3/ZnO@NH_2 showed a lower catalytic activity.

3.2.6 Role of hole and electron scavengers. The effect of various hole and electron scavengers was monitored in the photocatalytic preparation of chromene derivatives in the presence of the heterogeneous nanocatalyst WO_3/ZnO@NH_2-EY (Fig. 10). Generally, effective radical species such as hydroxyl radical, holes, and superoxide anion-radical are responsible for the photocatalytic reaction. Therefore, some familiar scavengers were separately included in the present reaction mixture. In these experiments, isopropyl alcohol (IPA) was employed to scavenge the hydroxyl free radical.[73] In this case, the yield% was decreased from 95 to 75%. In addition, a great decrease in the yield% (44%) in the presence of *p*-benzoquinone (BQ) (as an $^{\bullet}O_2^-$ scavenger)[74] proved that $^{\bullet}O_2^-$ would be involved in the reaction mechanism; therefore, O_2 strongly affects the photocatalytic process. Meanwhile, an 8% decrease in the yield% in the presence of ethylenediaminetetraacetic acid (EDTA) as an h^+ scavenger[75] also confirmed the possible contribution of h^+ in the photocatalytic reaction. As a result, reactive species such as $OH^{\bullet}$ and $^{\bullet}O_2^-$ along with h^+ were expected to be concerned in the present photocatalytic reaction.

3.2.7 Synthesis of different chromeno[4,3-*b*]chromene catalyzed by WO_3/ZnO@NH_2-EY. The versatility, limitations, and general scope of the present methodology were identified for the synthesis of a series of chromeno[4,3-*b*]chromene derivatives using a variety of aromatic aldehydes. Most of the performed aldehydes provided good to excellent yields in

Open Access Article. Published on 18 May 2021. Downloaded on 2/11/2026 11:12:10 PM.
This article is licensed under a Creative Commons Attribution-NonCommercial 3.0 Unported Licence.

a short period of time (Table 4). Aromatic aldehydes with different electron withdrawing/releasing substituents generated the desired products in good yields with superior selectivity. Although most of the electron-rich and electron-poor aldehydes afforded the desired products in high yields; however, in agreement with previous reports,[76,77] our experiments revealed that aldehyde-bearing electron-withdrawing groups react with better efficacy than those bearing electron-donating substituents.

3.2.8 Superiority of the present method over some reported catalysts. To date, a number of similar reports have accounted for the preparation of chromeno[4,3-*b*]chromene under different reaction conditions. The condensation yield of dimedone, benzaldehyde, and 4-hydroxycoumarin was contrasted with that reported in the literature, as shown in Table 5. In this experiment, the comparison was focused in terms of the most important experimental variables such as the reaction time, catalyst mol%, and yield%. Interestingly, the present methodology showed a few advantages using a very low amount of an environmental benign catalyst under mild reaction conditions and with an acceptable generality. Thus, this methodology is a special case, offering a new approach for the one-pot single-step preparation of the desired chromenes under milder conditions and, especially, under photochemical conditions with environment-friendly LED irradiation, which consumes a very low amount of electrical energy.

3.2.9 Studying the stability and reusability of WO_3/ZnO@NH_2-EY. To study the stability and reusability of WO_3/ZnO@NH_2-EY, the photocatalytic nanoparticles were removed after the completion of the first run by simple filtration. Then, the filtered catalyst was washed with a copious amount of toluene, well-dried at room temperature, and prepared for the next run. Therefore, the nanocatalyst was subsequently examined for four runs to prove its good stability and reusability (Fig. 11). This experiment revealed that the reactivity of the photocatalyst declined such that the yield% was decreased ~10% after the 4th run, which may be due to the poisoning of the catalyst surface or a little destruction of the photocatalyst framework. However, the comparison of the infrared spectra of WO_3/ZnO@NH_2-EY before and after the 4th run proved the existence of the main characteristic bands at about 1200–1800 cm^{-1}, assuring that the structure of WO_3/ZnO@NH_2 remained almost intact during the reaction (Fig. 12). In addition, typical experiments were repeated to warrant the reproducibility of the condensation reaction in the synthesis of chromeno[4,3-*b*]chromene and the acquired yields were repeatable with ±4% variation. Therefore, according to this experiment together with the consideration of the solvent-free conditions, it seems that the present protocol has some significant advantages compared to the reported protocols, especially with that of Singh *et al.*[83] The major improvements include the heterogeneity and recyclability of the catalyst.

3.2.10 Hot filtration test. The hot filtration test is recommended to ensure that the catalytic activity of the photocatalyst originates from the conjugated composite WO_3/ZnO@NH_2-EY and not from the drained segments, especially EY, in the reaction medium. Considering the high activity of EY in the preparation of chromeno[4,3-*b*]chromene, we specifically studied the leaching of this species from WO_3/ZnO@NH_2-EY. For this purpose, WO_3/ZnO@NH_2-EY (2 mg) was added to a mixture of dimedone, benzaldehyde, and 4-hydroxycoumarin, and the reaction was started under the standard conditions for 1.5 h. Then, the catalyst was separated off and the product yield of 58% was attained after removing the produced chromene. After that, the reaction was continued for another 1.5 h and the improved yield of 65% was attained based on the separated chromene. Interestingly, no further increase in the yield% was observed by prolonging the time to 5 h. Clearly, this experiment showed that an ~8% increase in the yield% should be due to the

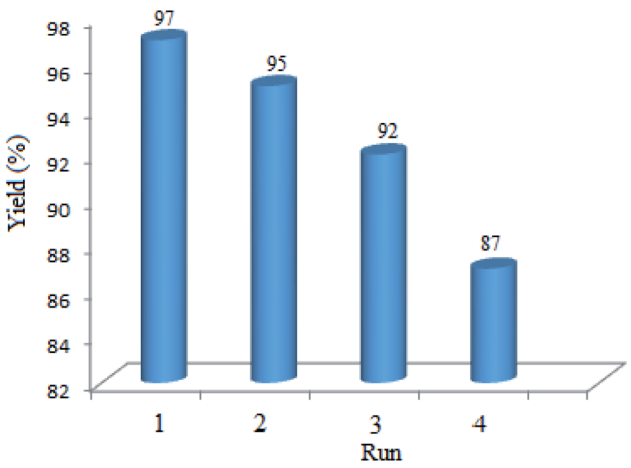

Fig. 11 Yield% as a function of the reusability of nano WO_3/ZnO@NH_2-EY.

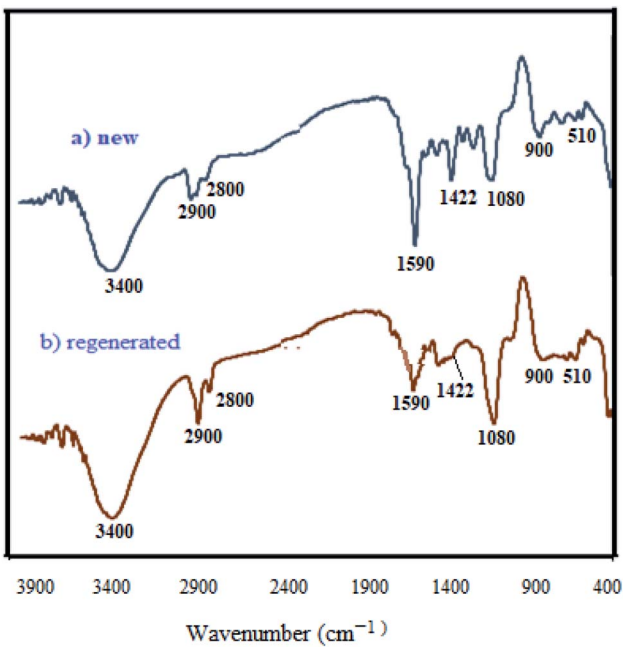

Fig. 12 FT-IR spectra of new (a) and regenerated (b) WO_3/ZnO@NH_2-EY.

© 2021 The Author(s). Published by the Royal Society of Chemistry

Open Access Article. Published on 18 May 2021. Downloaded on 2/11/2026 11:12:10 PM.
This article is licensed under a Creative Commons Attribution-NonCommercial 3.0 Unported Licence.

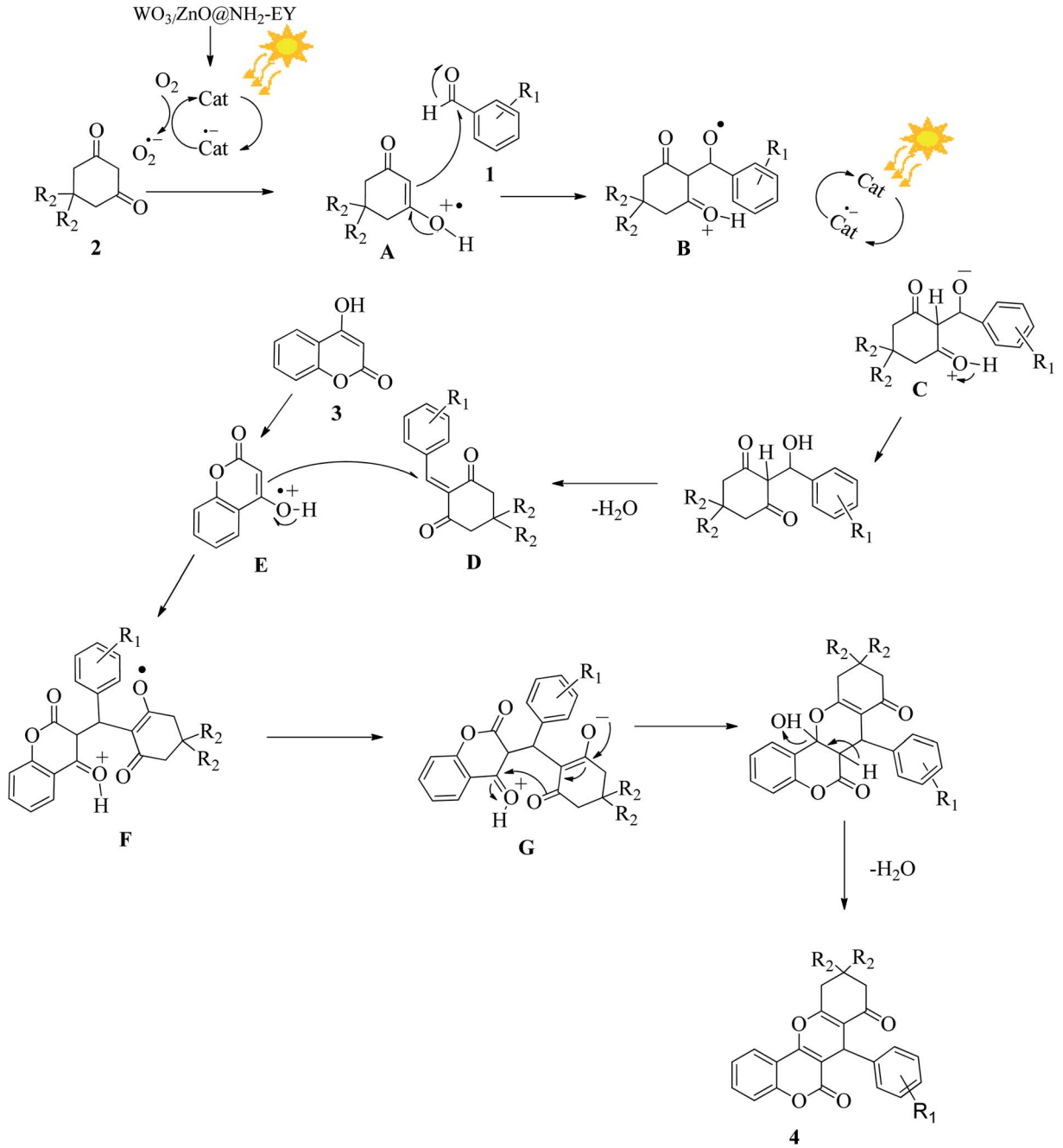

Fig. 13 A plausible reaction pathway for the fabrication of the desired chromene *via* consecutive electron transfer reactions.

leached EY or other fragments from the mother active nanocomposite WO_3/ZnO@NH_2-EY.

3.2.11 Suggesting a reasonable reaction pathway. On the basis of the literature survey,[58] a probable mechanism is illustrated in Fig. 13. Upon absorption of visible light, the photoredox catalyst can be converted into its excited state and provides a superoxide species to promote the conversion of the 1,3-dicarbonyl compound (2) into a radical cation (A). The generated radical cation (A) can interact with the aromatic aldehyde (1) to form an intermediate (B). Again, the photocatalyst participates in the reaction and facilitates the transformation of compound (B) to (C) *via* an electron transfer process. Eventually, the dehydration of compound (C) produces the β-dicarbonyl-enone (D), which can act as a Michael acceptor. Simultaneously, 4-hydroxycoumarin (3) can be converted into the radical-cation (E) *via* photochemical electron transfer and initiates a Michael-type addition reaction with β-dicarbonyl-enone (D) to furnish the desired compound (F). The continuation of the photochemical electron transfer reactions by the mediation of the nanophotocatalyst achieves the conversion of (F) into (G). Finally, (G) undergoes a simple

Open Access Article. Published on 18 May 2021. Downloaded on 2/11/2026 11:12:10 PM.
This article is licensed under a Creative Commons Attribution-NonCommercial 3.0 Unported Licence.

dehydration reaction and generates the target chromene product (4).

4 Conclusion

In conclusion, we have reported an ecofriendly and efficient method to achieve visible light-promoted synthesis of chromeno[4,3-*b*]chromenes under mild conditions. The photoredox catalyst WO_3/ZnO@NH_2-EY is used as a superior green alternative catalyst for the desired heterocyclic condensation reaction. The heterogeneous photoredox nanocatalyst was characterized by means of XRD, FT-IR, ICP, TGA, and SEM. The mild reaction conditions, wide substrate tolerance, solventless reactor, easy workup, high atom economy, cost-effectiveness, and good to excellent yields are the main features of this new photocatalytic system. The WO_3/ZnO@NH_2-EY nanocomposite exhibits its photocatalytic functions *via* a series of electron transfer reactions in the presence of visible light through a radical mechanism, as proven using various scavengers. This investigation showed that the reactive species such as $^{\bullet}O_2^-$ and $OH^{\bullet}$ along with h^+ are the main reactive species involved in the photochemical synthesis of chromenes. The WO_3/ZnO@NH_2-EY photocatalyst could be frequently recovered over four times without the loss of the catalytic activity. Eventually, a hot filtration test ensured that the nanohybrid catalyst is stable in the reaction mixture and its catalytic activity originates from the whole undecomposed nanocomposite.

Conflicts of interest

There are no conflicts to declare.

Acknowledgements

The authors/creators would like to acknowledge the financial support of Ministry of Science, Research and Technology for this project under grant number 12-99-02-000029. Also, the work has been supported by Hakim Sabzevari University.

References

1 R. C. Cioc, E. Ruijter and R. V. Orru, *Green Chem.*, 2014, **16**, 2958–2975.
2 M. B. Gawande, V. D. Bonifácio, R. Luque, P. S. Branco and R. S. Varma, *Chem. Soc. Rev.*, 2013, **42**, 5522–5551.
3 X. Guo and W. Hu, *Acc. Chem. Res.*, 2013, **46**, 2427–2440.
4 A. Dömling, *Chem. Rev.*, 2006, **106**, 17–89.
5 F. Wang, Y. Shen, H. Hu, X. Wang, H. Wu and Y. Liu, *J. Org. Chem.*, 2014, **79**, 9556–9566.
6 C. Simon, T. Constantieux and J. Rodriguez, *Eur. J. Org. Chem.*, 2004, **2004**, 4957–4980.
7 E. Ruijter, R. Scheffelaar and R. V. Orru, *Angew. Chem., Int. Ed.*, 2011, **50**, 6234–6246.
8 A. Amr, M. Abdalla, S. Essaouy, M. Areef, M. Elgamal, T. Nassear and A. Haschich, *Russ. J. Gen. Chem.*, 2017, **87**, 1826–1833.
9 S. W. Ng, L. H. Chung, C. F. Yeung, H. S. Lo, H. L. Shek, T. S. Kang, C. H. Leung, D. L. Ma and C. Y. Wong, *Chem.–Eur. J.*, 2018, **24**, 1779–1783.
10 W. H. Zhang, S. Chen, X. L. Liu, X. W. Liu and Y. Zhou, *Bioorg. Med. Chem. Lett.*, 2020, **30**, 127410.
11 I. V. Ilyina, O. S. Patrusheva, V. V. Zarubaev, M. A. Misiurina, A. V. Slita, I. L. Esaulkova, D. V. Korchagina, Y. V. Gatilov, S. S. Borisevich and K. P. Volcho, *Bioorg. Med. Chem. Lett.*, 2020, **31**, 127677.
12 N. Baral, D. R. Mishra, N. P. Mishra, S. Mohapatra, B. P. Raiguru, P. Panda, S. Nayak, M. Nayak and P. S. Kumar, *J. Heterocycl. Chem.*, 2020, **57**, 575–589.
13 A. Neghra, M. Lecsö, M. J. Butel, L. S. Espindola, B. Deguin and E. Seguin, *Nat. Prod. Commun.*, 2017, **12**, 1459–1463.
14 K. Haider, S. Rahaman, M. S. Yar and A. Kamal, *Expert Opin. Ther. Pat.*, 2019, **29**, 623–641.
15 I. Zghab, B. Trimeche, M. B. Mansour, M. Hassine, D. Touboul and H. B. Jannet, *Arabian J. Chem.*, 2017, **10**, S2651–S2658.
16 F. Borges, F. Roleira, N. Milhazes, L. Santana and E. Uriarte, *Curr. Med. Chem.*, 2005, **12**, 887–916.
17 M. Mahdavi, J. Davoodi, M. R. Zali and A. Foroumadi, *Biomed. Pharmacother.*, 2011, **65**, 175–182.
18 J.-L. Wang, D. Liu, Z.-J. Zhang, S. Shan, X. Han, S. M. Srinivasula, C. M. Croce, E. S. Alnemri and Z. Huang, *Proc. Natl. Acad. Sci., India*, 2000, **97**, 7124–7129.
19 S. A. Patil, J. Wang, X. S. Li, J. Chen, T. S. Jones, A. Hosni-Ahmed, R. Patil, W. L. Seibel, W. Li and D. D. Miller, *Bioorg. Med. Chem. Lett.*, 2012, **22**, 4458–4461.
20 A. M. Shestopalov, Y. M. Litvinov, L. A. Rodinovskaya, O. R. Malyshev, M. N. Semenova and V. V. Semenov, *ACS Comb. Sci.*, 2012, **14**, 484–490.
21 G. A. Kraus and I. Kim, *J. Org. Chem.*, 2003, **68**, 4517–4518.
22 J. G. Tangmouo, A. L. Meli, J. Komguem, V. Kuete, F. N. Ngounou, D. Lontsi, V. P. Beng, M. I. Choudhary and B. L. Sondengam, *Tetrahedron Lett.*, 2006, **47**, 3067–3070.
23 R. O. S. Kitamura, P. Romoff, M. C. M. Young, M. J. Kato and J. H. G. Lago, *Phytochemistry*, 2006, **67**, 2398–2402.
24 M. Kamali, *Synth. Commun.*, 2020, **51**, 1–9.
25 H. Anaraki-Ardakani, *Russ. J. Gen. Chem.*, 2017, **87**, 1820–1825.
26 H. Emtiazi and M. A. Amrollahi, *S. Afr. J. Chem.*, 2014, **67**, 175–179.
27 F. Khosravian, B. Karami and M. Farahi, *New J. Chem.*, 2017, **41**, 11584–11590.
28 H. Anaraki-Ardakani, R. Ghanavatian and M. Akbari, *World Appl. Sci. J.*, 2013, **22**, 802–808.
29 S. Vajar and M. Mokhtary, *Polycyclic Aromat. Compd.*, 2019, **39**, 111–123.
30 X.-J. Sun, J.-F. Zhou and S.-J. Zhi, *Synth. Commun.*, 2012, **42**, 1987–1994.
31 R. Tayebee, A. Pejhan, H. Ramshini, B. Maleki, N. Erfaninia, Z. Tabatabaie and E. Esmaeili, *Appl. Organomet. Chem.*, 2018, **32**, e3924.
32 B. Maleki, S. Babaee and R. Tayebee, *Appl. Organomet. Chem.*, 2015, **29**, 408–411.

© 2021 The Author(s). Published by the Royal Society of Chemistry

Open Access Article. Published on 18 May 2021. Downloaded on 2/11/2026 11:12:10 PM. This article is licensed under a Creative Commons Attribution-NonCommercial 3.0 Unported Licence.

33 S. K. Sahoo, *Renewable Sustainable Energy Rev.*, 2016, **59**, 927–939.
34 A. Juris, V. Balzani, F. Barigelletti, S. Campagna, P. L. Belser and A. V. von Zelewsky, *Coord. Chem. Rev.*, 1998, **84**, 85–277.
35 P. Melchiorre, *Angew. Chem., Int. Ed.*, 2009, **48**, 1360–1363.
36 D. A. Nagib, M. E. Scott and D. W. MacMillan, *J. Am. Chem. Soc.*, 2009, **131**, 10875–10877.
37 M. A. Ischay, Z. Lu and T. P. Yoon, *J. Am. Chem. Soc.*, 2010, **132**, 8572–8574.
38 Y. Zhang, C. Ye, S. Li, A. Ding, G. Gu and H. Guo, *RSC Adv.*, 2017, **7**, 13240–13243.
39 V. Srivastava and P. P. Singh, *RSC Adv.*, 2017, **7**, 31377–31392.
40 D. P. Hari and B. König, *Chem. Commun.*, 2014, **50**, 6688–6699.
41 S. Yadav, M. Srivastava, P. Rai, B. P. Tripathi, A. Mishra, J. Singh and J. Singh, *New J. Chem.*, 2016, **40**, 9694–9701.
42 N. Hashim, S. Thakur, M. Patang, F. Crapulli and A. K. Ray, *Environ. Technol.*, 2017, **38**, 933–944.
43 G. Kumar, P. Solanki, M. Nazish, S. Neogi, R. I. Kureshy and H. K. Noor-ul, *J. Catal.*, 2019, **371**, 298–304.
44 S. Gazi and R. Ananthakrishnan, *Appl. Catal., B*, 2011, **105**, 317–325.
45 A. Sridhar, R. Rangasamy and M. Selvaraj, *New J. Chem.*, 2019, **43**, 17974–17979.
46 P. Li, G.-W. Wang, X. Zhu and L. Wang, *Tetrahedron*, 2019, **75**, 3448–3455.
47 L. Wang, S. Yue, Q. Zhang, Y. Zhang, Y. R. Li, C. S. Lewis, K. J. Takeuchi, A. C. Marschilok, E. S. Takeuchi and S. S. Wong, *ACS Energy Lett.*, 2017, **2**, 1465–1478.
48 R. Celiesiute, A. Ramanaviciene, M. Gicevicius and A. Ramanavicius, *Crit. Rev. Anal. Chem.*, 2019, **49**, 195–208.
49 X. Yu, T. J. Marks and A. Facchetti, *Nat. Mater.*, 2016, **15**, 383–396.
50 A. K. Arora, V. S. Jaswal, K. Singh and R. Singh, *Orient. J. Chem.*, 2016, **32**, 2035.
51 M. J. Limo, A. Sola-Rabada, E. Boix, V. Thota, Z. C. Westcott, V. Puddu and C. C. Perry, *Chem. Rev.*, 2018, **118**, 11118–11193.
52 M. B. Tahir, G. Nabi and N. Khalid, *Mater. Sci. Semicond. Process.*, 2018, **84**, 36–41.
53 E. Mugunthan, M. Saidutta and P. Jagadeeshbabu, *J. Photochem. Photobiol., A*, 2019, **383**, 111993.
54 F. Akhlaghian and A. Najafi, *Sci. Iran.*, 2018, **25**, 3345–3353.
55 N. Geetha, S. Sivaranjani, A. Ayeshamariam, M. K. Micheal, D. Saravankkumar, S. Fowziya, A. Mohideen and M. Jayachandran, *J. Adv. Microsc. Res.*, 2018, **13**, 3–11.
56 Z. Xiong, Z. Lei, Z. Xu, X. Chen, B. Gong, Y. Zhao, H. Zhao, J. Zhang and C. Zheng, *J. CO_2 Util.*, 2017, **18**, 53–61.
57 B. Maleki, H. Natheghi, R. Tayebee, H. Alinezhad, A. Amiri, S. A. Hossieni and S. M. M. Nouri, *Polycyclic Aromat. Compd.*, 2020, **40**, 633–643.
58 B. Maleki, M. Chahkandi, R. Tayebee, S. Kahrobaei, H. Alinezhad and S. Hemmati, *Appl. Organomet. Chem.*, 2019, **33**, e5118.
59 R. Tayebee, M. Fattahi Abdizadeh, N. Erfaninia, A. Amiri, M. Baghayeri, R. M. Kakhki, B. Maleki and E. Esmaili, *Appl. Organomet. Chem.*, 2019, **33**, e4959.
60 H. Zhao, X. Liu, Z. Cao, Y. Zhan, X. Shi, Y. Yang, J. Zhou and J. Xu, *J. Hazard. Mater.*, 2016, **310**, 235–245.
61 Y. Liu, J. Xu, Z. Cao, R. Fu, C. Zhou, Z. Wang and X. Xu, *J. Colloid Interface Sci.*, 2020, **559**, 215–225.
62 X. Liu, J. Xu, Y. Zhao, H. Shi and C.-H. Huang, *Chemosphere*, 2019, **226**, 726–735.
63 J. Xu, Z. Cao, Y. Zhang, Z. Yuan, Z. Lou, X. Xu and X. Wang, *Chemosphere*, 2018, **195**, 351–364.
64 K. S. Babu, A. R. Reddy, C. Sujatha, K. V. Reddy and A. Mallika, *J. Adv. Ceram.*, 2013, **2**, 260–265.
65 B. Li, R. Tayebee, E. Esmaeili, M. S. Namaghi and B. Maleki, *RSC Adv.*, 2020, **10**, 40725–40738.
66 X. Z. Yajun Wang, L. Duan, F. Wang, H. Niu, W. Guo and A. Ali, *Mater. Sci. Semicond. Process.*, 2015, **29**, 372–379.
67 D. Jaiswal, A. Mishra, P. Rai, M. Srivastava, B. P. Tripathi, S. Yadav, J. Singh and J. Singh, *Res. Chem. Intermed.*, 2018, **44**, 231–246.
68 D. A. Young, T. B. Freedman, E. D. Lipp and L. A. Nafie, *J. Am. Chem. Soc.*, 1986, **108**, 7255–7263.
69 A. Chiolerio, A. Chiodoni and P. Allia, *Thin Solid Films*, 2008, **516**, 8453–8461.
70 F. Liu, X. Chen, Q. Xia, L. Tian and X. Chen, *RSC Adv.*, 2015, **5**, 77423–77428.
71 H. Alinezhad, M. Tarahomi, B. Maleki and A. Amiri, *Appl. Organomet. Chem.*, 2019, **33**, e4661.
72 V. Kandathil, B. D. Fahlman, B. Sasidhar, S. A. Patil and S. A. Patil, *New J. Chem.*, 2017, **41**, 9531–9545.
73 R. K. Sharma, B. Arora, S. Sharma, S. Dutta, A. Sharma, S. Yadav and K. Solanki, *Mater. Chem. Front.*, 2020, **4**, 605–620.
74 Z. Yin, M. Han, Z. Hu, L. Feng, Y. Liu, Z. Du and L. Zhang, *Chem. Eng. J.*, 2020, **390**, 124532.
75 X. Zheng, J. Yuan, J. Shen, J. Liang, J. Che, B. Tang, G. He and H. Chen, *J. Mater. Sci.: Mater. Electron.*, 2019, **30**, 5986–5994.
76 K. Pradhan, S. Paul and A. R. Das, *Tetrahedron Lett.*, 2013, **54**, 3105–3110.
77 F. Adibian, A. R. Pourali, B. Maleki, M. Baghayeri and A. Amiri, *Polyhedron*, 2020, **175**, 114179.
78 Z. Chen, Q. Zhu and W. Su, *Tetrahedron Lett.*, 2011, **52**, 2601–2604.
79 K. T. Patil, L. Walekar, S. Undare, G. Kolekar, M. B. Deshmukh, P. Choudhari and P. V. Anbhule, *Indian J. Chem.*, 2016, **55**, 1151–1159.
80 A. Shafiee, R. Motamedi, O. Firuzi, S. Meili, A. R. Mehdipour and R. Miri, *Med. Chem. Res.*, 2011, **20**, 466–474.
81 R. Motamedi, S. Baghbani and F. F. Bamoharram, *Synth. Commun.*, 2012, **42**, 1604–1612.
82 A. Saha, S. Payra and S. Banerjee, *RSC Adv.*, 2015, **5**, 101664–101671.
83 A. K. Sharma, J. Tiwari, D. Jaiswal, S. Singh, J. Singh and J. Singh, *Curr. Organocatal.*, 2019, **6**, 222–230.